Uniform hexagonal graphene flakes and films grown on liquid copper surface

Dechao Geng[1], Bin Wu[1], Yunlong Guo, Liping Huang, Yunzhou Xue, Jianyi Chen, Gui Yu, Lang Jiang, Wenping Hu, and Yunqi Liu[2]

Beijing National Laboratory for Molecular Sciences, Key Laboratory of Organic Solids, Institute of Chemistry, Chinese Academy of Sciences, Beijing 100190, People's Republic of China

Unresolved problems associated with the production of graphene materials include the need for greater control over layer number, crystallinity, size, edge structure and spatial orientation, and a better understanding of the underlying mechanisms. Here we report a chemical vapor deposition approach that allows the direct synthesis of uniform single-layered, large-size (up to 10,000 μm^2), spatially self-aligned, and single-crystalline hexagonal graphene flakes (HGFs) and their continuous films on liquid Cu surfaces. Employing a liquid Cu surface completely eliminates the grain boundaries in solid polycrystalline Cu, resulting in a uniform nucleation distribution and low graphene nucleation density, but also enables self-assembly of HGFs into compact and ordered structures. These HGFs show an average two-dimensional resistivity of $609 \pm 200\ \Omega$ and saturation current density of $0.96 \pm 0.15\ mA/\mu m$, demonstrating their good conductivity and capability for carrying high current density.

atomic crystal | electronic materials

Graphene has attracted considerable attention because of its extraordinary physical properties and potential electronic and spintronic applications (1–3). It is critical to find ways of precisely controlling the graphene layer number (4–6), crystallinity, size, edge structure, and even spatial orientation. The chemical vapor deposition (CVD) approach is a powerful and cost-effective technique for the production of high-quality and large-scale graphene films. In spite of the complexity of CVD procedures involving different catalysts, carbon sources, and other variables, the physical principles underlying this method are relatively simple. It is widely accepted that CVD mainly involves either surface catalytic reaction (7, 8) or bulk carbon precipitation onto the surface during cooling (9, 10) for catalysts with low-carbon and high-carbon solubility, respectively. In both cases, graphene nucleation on a catalyst surface is one of the critical steps in the growth process. Various factors affect the initiation of the graphene nucleation process, including the type (11, 12) or surface microstructure of the catalyst, carbon source (13), carbon segregation from metal-carbon melts (14), processing history, and parameters in CVD growth (15–17). In general, nucleation densities on substrates such as Cu or Ni are nonuniform. This nonuniformity causes a large dispersion of both nucleus density and size distribution of graphene, representing a general problem in graphene CVD growth systems.

It has been found that low-pressure CVD synthesis of graphene on Cu foil provides a good way of fabricating uniform single-layer graphene films (7). Studies have shown that the continuous films were formed by connecting randomly oriented, irregular-shaped, and micrometer-sized graphene flakes, resulting in the presence of a large amount of both low- and high-angle grain boundaries composed of pentagons and heptagons, which leads to a dramatic degradation in electronic properties compared with those of pristine graphene (7, 18–20). Recently, we (21) and others (22, 23) have shown that it is possible to grow single-crystalline hexagonal graphene flakes (HGFs) with a predominance of zigzag edges at ambient pressure by controlling the growth rate of graphene. The HGF is an ideal building block for the construction of continuous graphene films and allows study of their edge/orientation-dependent physics. The layer number of HGFs was found to be strongly influenced by the gas flow ratio of Ar to H_2, an increase of which led to a change from mixed single/multilayer to single-layer-dominated HGFs, consistent with previous results (24). However, graphene nucleation preferentially occurs on high-surface energy locations such as grain boundaries or defects associated with solid polycrystalline Cu, resulting in HGFs with inhomogeneous density and size distribution. In addition, the high graphene nucleation density and the observed slow growth rate of HGFs result in an HGF size typically in the range of 1–10 μm in the diagonal direction (21–23). Here we demonstrate that the use of liquid Cu is a particularly effective means for controlling the nucleation process in graphene CVD systems because it eliminates the grain boundaries found in solid Cu and results in the production of uniform single-layered, self-aligned, large-sized, single-domain HGFs and continuous monolayer films.

Results and Discussion

The approach involves the formation of liquid Cu phase on quartz and W substrates at the growth temperature above Cu melting point (Fig. S1). Fig. 1 *A* and *B* shows typical SEM images of well-dispersed HGFs grown on liquid Cu spheres on a quartz substrate. Raman measurements of HGFs (Fig. 1*D*) on the Cu surface show the typical characteristics (25) of monolayer graphene—namely a large I_{2D}/I_G intensity ratio (~2.5–4) of the two-dimensional (2D) and G bands, a symmetric 2D peak located at 2,698 cm^{-1} with FWHM of 35–40 cm^{-1}—consistent with uniform contrast observed in Fig. 1 *A–C*. The yield of monolayer HGFs was very high, with the formation of only a few bilayer or trilayer HGFs (Fig. S2 *A–C*). Importantly, these HGFs also formed well-distributed assemblies on the surface of Cu spheres. The dynamic changes in density and size of HGFs on Cu spheres were monitored as shown in Fig. S2 *D–F*. The spatial arrangement of HGFs on Cu spheres was uniform in all cases with the average size of HGFs being about 5 μm, and the average distance between HGFs decreasing with increasing growth time. These results are consistent with surface nucleation and growth mechanism in the case of growing graphene on solid Cu.

This approach of HGFs formed on flat liquid Cu/W surface is illustrated in Fig. 2*A*, and these HGFs displayed similar features
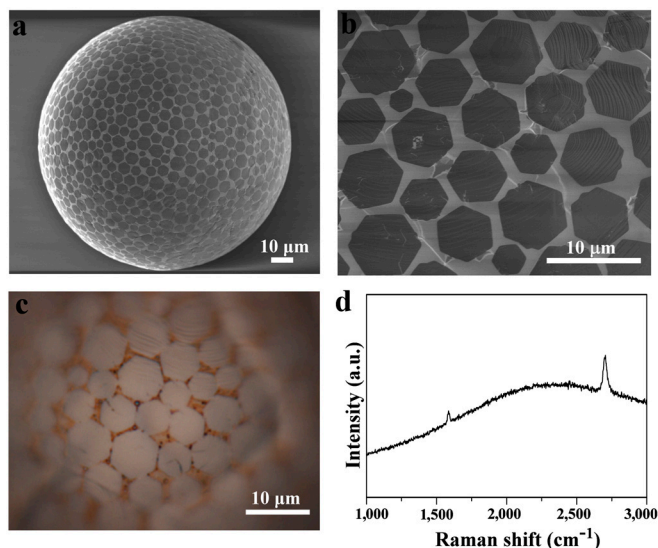
Fig. 1. The growth of HGFs on liquid Cu spheres/quartz substrate. (A) Typical SEM image showing well-dispersed, self-aligned HGFs on the surface of Cu spheres grown using 10 sccm CH$_4$/300 sccm H$_2$ at 1,080 °C for 20 min. (B) The corresponding magnified SEM image. (C) Optical image of HGFs on Cu spheres showing the color contrast between separated HGFs and the Cu surface, indicating the single-layer nature of the HGFs. (D) Typical Raman spectrum of an HGF confirming its single-layer characteristics.

with the above Cu sphere system. Typically, HGFs were well-dispersed on the surface, and there was no clear alignment relation between different HGFs when the HGFs were not fully covering the surface (Fig. 2B, Fig. S3A). As the density or coverage of HGFs on the Cu surface increased, introducing spatial constraint of the HGFs, the HGFs became self-aligned into an ordered structure with the most compact packing arrangement (Fig. 2C), mimicking the polycrystalline structure in metals. The edge-to-edge alignment of HGFs led to the formation of low-angle grain boundaries for adjacent HGFs. Remarkably, perfectly ordered

2D lattice structures of HGFs were obtained when the HGFs possessed similar size (Fig. 2D). These observations indicate that the translation or rotation of HGFs on a liquid Cu surface is involved in the self-assembly of their ordered structures, and the minimization of total HGF surface/edge energy on liquid Cu surface may be responsible for the alignment.

The evolution from well-separated HGFs, to closely packed structures, to continuous film is a direct result of the extended nucleation and growth in the CVD system. We found that growth for 40 min produced continuous monolayer graphene films, and similar results were obtained with longer growth times (for example, from 1–4 h). Fig. 2E shows a typical SEM image of a large area of continuous graphene film grown for 2 h. The shape and edges of the HGFs disappeared, and the appearance of the film in images was similar to those grown at low pressure, as shown in Fig. S3 B and C. Raman measurements were also performed on many points of this film, and almost all of them exhibited a single-layer nature, consistent with SEM and optical measurements.

The average size of individual HGFs is determined by both nucleation density and growth rate. Typical average size in Fig. 2 B–D is about 20–30 μm. Increasing growth temperature reproducibly leads to HGFs with average sizes of approximately 50 μm; and lowering CH$_4$ flow rate leads to approximately 120 μm, as shown in Fig. 2 F and G, respectively. This large size is a reflection of low nucleation density of HGFs in the liquid Cu CVD system. The average growth rate of HGFs was estimated to be 10–50 μm/min on flat Cu/W, which is much higher than the rate of 0.1–0.2 μm/min observed for the case of HGFs grown on a Cu solid surface (21). This result is highly important as it shows that a liquid Cu surface favors the fast growth rate of graphene without compromising its unique shape, highlighting the possibility of realizing macroscopic-sized HGFs that are otherwise difficult to achieve with slow growth.

Several differences were revealed between HGFs grown on liquid and solid Cu surfaces. Although the latter produces a mixture of single- and multilayer HGFs, small size, an inhomogeneous spatial dispersion, and random orientation, the former results in HGFs with uniform single-layer characteristics, large size, well-dispersed configurations, and a clear orientation rela-
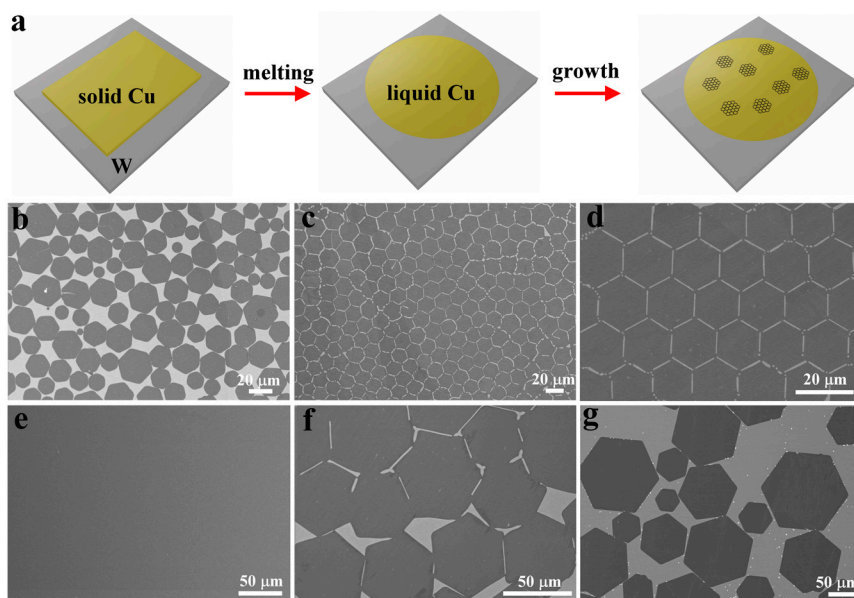
Fig. 2. The growth of HGFs on flat liquid Cu surfaces on W substrates. (A) Scheme showing CVD process for the synthesis of HGFs on liquid Cu surface. (B) SEM image showing partially covered and well-dispersed HGFs using 6 sccm CH$_4$/300 sccm H$_2$ at 1,120 °C for 30 min. (C) SEM image of HGFs showing a compact assembly of HGFs in which the dark and bright parts represent HGFs and the Cu surface, respectively. (D) SEM image of a near-perfect 2D lattice composed of similar-sized HGFs. (E) SEM image of the sample for 2 h growth showing the continuous graphene film with uniform contrast. (F and G) SEM images of large-sized HGFs showing that the average sizes are approximately 50 μm and approximately 120 μm using 1,140 °C and 1,160 °C, respectively. Experimental conditions from C and D are the same, using 6 sccm CH$_4$/300 sccm H$_2$ at 1,120 °C for 38 min.
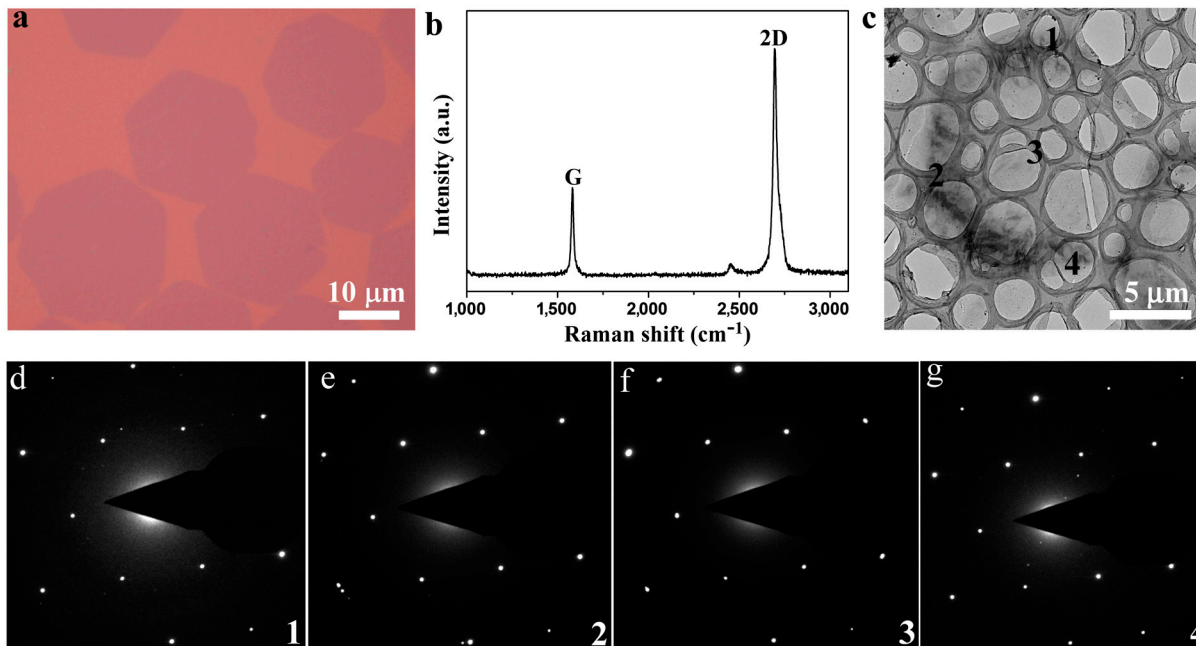
Fig. 3. Raman and TEM characterizations. (*A*) Typical optical image of HGFs transferred onto 300 nm SiO$_2$/Si substrate. (*B*) Typical Raman spectroscopy of thus-transferred HGFs showing single-layer characteristics of HGFs and no detectable D-band. (*C*) Low-magnification TEM image showing an individual HGF. (*D*–*G*) Selected area electron diffraction data for small regions indicated **1** to **4**. These SAED data confirm the single-crystalline structure of the HGF as they show the same set of sixfold symmetric diffraction points.

tion between different HGFs. These differences correlated well with dramatic differences between the surface properties of liquid and solid Cu. First, a liquid Cu surface completely eliminates the grain boundaries, resulting in a low nucleation density (i.e., large size) and more homogeneous nucleation on surface compared to using solid Cu. The subsequent grain growth of HGF nuclei is also uniform in all directions as indicated by the formation of regular-shaped HGFs instead of equiangular-shaped HGFs, possibly due to anisotropic solid Cu lattice. Second, liquid Cu surface provides a higher C atom diffusion rate, favoring the fast
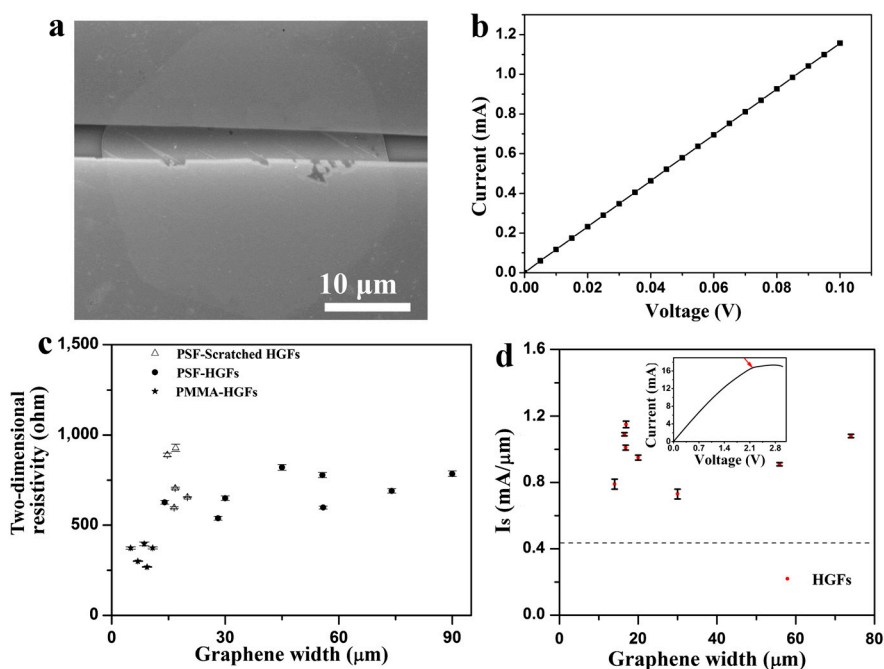

Fig. 4. Electrical characterization of HGFs. (*A*) SEM image of one typical two-terminal device based on an individual HGF contacted by 30 nm top and bottom gold electrodes. (*B*) The corresponding I–V curve of the device with a resistance and 2D resistivity values of approximately 87 Ω and 650 Ω, respectively. (*C*) A plot of 2D resistivity of HGFs as a function of graphene width in many devices, in which transfer material, treatment, and graphene under tests are indicated, with PSF-scratched HGFs for comparison. (*D*) A plot of saturation current density (I$_s$) vs. HGF width measured for many devices. The dashed line indicates the value of 0.44 mA/μm for CVD-grown graphene from ref. 28. (*Inset*) The I–V curve of an HGF device with a width of 16.8 μm showing the current saturation behavior. Note that the I–V curve becomes nonlinear at high current in this case. The arrow indicates the turning point of the current and is used to calculate the saturation current density.

growth of HGFs that is one of the critical factors responsible for large size. Third, the floating HGFs on liquid Cu surface self-assemble into a compact, ordered structure. This alignment of HGFs is difficult to realize in solid Cu surfaces, as the epitaxial alignment of HGFs brought about by a solid Cu lattice is weak (21, 23). Finally, the production of dominated single-layer HGFs is also exceptional, as using similar experimental conditions to grow HGFs on solid Cu mainly resulted in significant amounts of multilayer HGFs characterized by a central dark area in SEM or optical images (21, 22). We speculate that the high mobility of Cu atoms in the liquid state may erase the nucleation vacancies, preventing growth of a second layer on the same nucleus. Control experiments were further performed to illustrate the role of the liquid Cu phase (Fig. S4, Fig. S5).

HGFs were transferred onto 300 nm SiO_2/Si substrate (Fig. 3A) and transmission electron microscopy (TEM) grid for Raman spectroscopy and crystalline structure characterizations using poly (methyl methacrylate) (PMMA) or polysulfone (PSF) supporting layers (see *Methods*). The shape and position of peaks, and the intensity ratio between 2D and G peaks, confirmed the single-layer nature (Fig. 3B) (25). Twelve individual HGFs with different sizes were tested by selected area electron diffraction (SAED) on different locations of each HGF. The single-crystal-line nature of all 12 HGFs was confirmed by the observations of the same set of sixfold symmetric diffraction spots at different locations (the maximum distance between two locations was about 45 μm, Fig. S6), as shown in Fig. 3 C–G.

We fabricated field-effect transistor (FET) devices using individual HGFs transferred onto 300 nm SiO_2/Si substrates. More than 90% of the devices showed linear and reproducible I–V curves, demonstrating the ohmic contact obtained between HGFs and Au electrodes using our device fabrication method (21, 26). Fig. 4 A and B show a typical SEM image of a single-layer HGF device together with its current-voltage (I–V) curve measured under ambient conditions (see more cases in Fig. S7). The resistance of the device is approximately 87 Ω. Fig. 4C shows a plot of 2D HGF resistivity (defined as $R \times W/L$, where W is the width of the HGF, L is the channel length of the device, and R is the resistance) as a function of HGF width. The average value of 2D resistivity of the HGFs is 609 ± 200 Ω approaching approximately 230 Ω for pristine peel-off graphene (27). Importantly, measurements were also taken on several small PSF-scratched HGFs that were obtained by cutting large-width PSF-HGFs. The 2D resistivity showed no dependence on the width of HGFs, showing that the electrical properties of large HGFs are microscopically uniform.

We also observed clear current saturation in all measured devices, as shown in Fig. 4D and its *Inset*, as has also been recently observed for CVD-grown graphene with long channel lengths (28). Large saturation current densities (defined as saturation current divided by graphene device width) were found from I–V curves of these two-terminal devices. The value of the saturation current for the HGFs was 0.96 ± 0.15 mA/μm, approximately twice that (0.44 mA/μm) for CVD-grown graphene (28), indicating its capability of carrying high current density. It should be mentioned that HGFs grown on solid Cu have similar values of both 2D resistivity and saturation current density with those grown on liquid Cu. In addition, FET measurements were also performed on these devices, and the average hole mobility values in HGF devices fell into a range (1,000–2,500 cm^2 V^{-1} s^{-1}), consistent with that of HGFs grown on a solid Cu surface (21, 29) and those of the typical results (7, 13, 15, 30–32) for graphene produced on Cu (Fig. S7, Fig. S8, Table S1).

Conclusions

In summary, we have demonstrated that the use of liquid Cu is a particularly effective means for controlling the nucleation process in graphene CVD systems, and results in the production of uniform single-layered, self-aligned, large-sized, single-domain HGFs and continuous monolayer films. The combined data of Raman spectra, TEM, and electrical tests reveal a single-crystalline nature, reasonable carrier mobility, high conductivity, and the capability for carrying a large current of HGFs grown on liquid Cu surface.

Methods

Materials. Cu foils (99.8% purity) that were 25-μm thick and 50-m thick W foils (99.95%) were obtained from Alfa Aesar. One to three pieces of Cu foils were directly placed onto quartz substrates, and various-sized liquid Cu spheres were formed on the quartz surface during the high-temperature annealing process due to the nonwetting nature between Cu and quartz. Similarly, two to four pieces of Cu foil were directly put on W foil for growing HGFs on a flat liquid Cu surface. Electroplated Cu films on W substrates from $CuSO_4$ aqueous solution (256 g/L) were also used.

CVD Graphene Synthesis and Transfer. Prior to graphene growth, the CVD 2.54-cm quartz tube was pumped to approximately 5 Pa to clean the system, and then filled with 200 standard cubic cm per min (sccm) H_2 followed by heating the furnace (Lindberg/Blue M, TF55035A) to the desired temperature above the melting point of Cu over 30–40 min. Subsequently, annealing for 30 min was employed. In the case of Cu spheres on quartz substrates, different temperatures and annealing times were employed to study the growth mechanism and the relationship between experimental conditions and the properties of the resulting HGF (Fig. S4). In each case, changing temperature was realized by simply switching off the furnace, and the temperature dropped from 1,080 °C to desired one in about 2–4 min. Then the furnace was turned on until the desired temperature was obtained. At the beginning of growth, the H_2 flow rate was changed to the desired value, and CH_4 was then introduced to the chamber with the required value for a certain time. Finally, CH_4 was turned off, and the system was cooled down to room temperature at the cooling rate of about 25 °C/min. In the case of Cu on W foil, after the annealing process, typical growth conditions were 6 sccm CH_4 and 300 sccm H_2 at 1,120 °C for 28 min to 4 h. In this case of 28 min growth, no HGFs were grown. This fact was used to evaluate HGF growth rate. The experimental parameters are described in the corresponding figure captions for each case. Note that there is no observable Cu deposition on the quartz tube after many runs of graphene growth, consistent with low vapor pressure of liquid Cu (~0.05 Pa at 1,120 °C). The HGFs grown on flat Cu/W surfaces were also transferred to 300 nm SiO_2/Si substrates and TEM grids by PMMA-assisted or PSF (average molecular weight 22,000), assisted methods similar to those reported previously. PMMA and PSF supporting films were removed by acetone and chloroform rinsing, respectively.

Characterization of HGFs. The samples were characterized by SEM (Hitachi S-4800, 1 kV and 15 kV), optical microscopy, Raman spectroscopy (Renishaw Invia plus, with laser excitation of 514 nm and spot size of 1–2 μm), and TEM (Tecnai G2 F20 U-TWIN, operated at 200 kV).

Device Fabrication and Electrical Properties of HGFs and Films. The electrical properties of HGFs were measured after they were transferred onto 300 nm SiO_2/Si substrates. FET devices based on HGFs were fabricated using our previous method (21, 26). Briefly, 2–5-μm wide nanowires (a rigid H type anthracene derivative) (26) were deposited on individual HGFs, and then a 30 nm gold film was evaporated on the sample. Finally, the nanowires were removed by a micromanipulator, and the desired electrodes were fabricated by mechanically scratching the gold film to make isolated FET devices. The tests, including measuring I–V curves and back-gated FET properties of HGFs, were conducted with a Keithley 4200 analyzer at room temperature in air, and 2D resistivity and saturation current density for HGFs were calculated from the data. The mobility of charge carriers is extracted from the equation $\mu_{dev} = \frac{L}{V_D C_{ox} W} \cdot \frac{dI_d}{dV_g}$, where L and W are the device channel length and width, V_D is the voltage between source and drain electrodes, and C_{ox} is the gate capacitance per unit area.

1. Novoselov KS, et al. (2004) Electric field effect in atomically thin carbon films. *Science* 306:666–669.
2. Geim AK, Novoselov KS (2007) The rise of graphene. *Nat Mater* 6:183–191.
3. Geim AK (2009) Graphene: Status and prospects. *Science* 324:1530–1534.
4. Yan Z, et al. (2011) Growth of bilayer graphene on insulating substrates. *ACS Nano* 5:8187–8192.
5. Lee S, Lee K, Zhong Z (2010) Wafer scale homogeneous bilayer graphene films by chemical vapor deposition. *Nano Lett* 10:4702–4707.
6. Yan K, Peng HL, Zhou Y, Li H, Liu ZF (2011) Formation of bilayer Bernal graphene: Layer-by-layer epitaxy via chemical vapor deposition. *Nano Lett* 11:1106–1110.
7. Li XS, et al. (2009) Large-area synthesis of high-quality and uniform graphene films on copper foils. *Science* 324:1312–1314.
8. Li XS, Cai WW, Colombo L, Ruoff RS (2009) Evolution of graphene growth on Ni and Cu by carbon isotope labeling. *Nano Lett* 9:4268–4272.
9. Kim KS, et al. (2009) Large-scale pattern growth of graphene films for stretchable transparent electrodes. *Nature* 457:706–710.
10. Reina A, et al. (2009) Large area, few-layer graphene films on arbitrary substrates by chemical vapor deposition. *Nano Lett* 9:30–35.
11. Sutter PW, Flege JI, Sutter EA (2008) Epitaxial graphene on ruthenium. *Nat Mater* 7:406–411.
12. Gao L, Guest JR, Guisinger NP (2010) Epitaxial graphene on Cu(111). *Nano Lett* 10:3512–3516.
13. Sun ZZ, et al. (2010) Growth of graphene from solid carbon sources. *Nature* 468:549–552.
14. Amini S, Garay J, Liu GX, Balandin AA, Abbaschian R (2010) Growth of large-area graphene films from metal-carbon melts. *J Appl Phys* 108:094321.
15. Li XS, et al. (2011) Large-area graphene single crystals grown by low-pressure chemical vapor deposition of methane on copper. *J Am Chem Soc* 133:2816–2819.
16. Bae S, et al. (2010) Roll-to-roll production of 30-inch graphene films for transparent electrodes. *Nat Nanotechnol* 5:574–578.
17. Bhaviripudi S, Jia XT, Dresselhaus MS, Kong J (2010) Role of kinetic factors in chemical vapor deposition synthesis of uniform large area graphene using copper catalyst. *Nano Lett* 10:4128–4133.
18. Kim K, et al. (2011) Grain boundary mapping in polycrystalline graphene. *ACS Nano* 5:2142–2146.
19. Huang PY, et al. (2011) Grains and grain boundaries in single-layer graphene atomic patchwork quilts. *Nature* 469:389–392.
20. Yazyev OV, Louie SG (2010) Electronic transport in polycrystalline graphene. *Nat Mater* 9:806–809.
21. Wu B, et al. (2011) Equilangular hexagon-shape-controlled synthesis of graphene on copper surface. *Adv Mater* 23:3522–3525.
22. Robertson AW, Warner JH (2011) Hexagonal single crystal domains of few-layer graphene on copper foils. *Nano Lett* 11:1182–1189.
23. Yu QK, et al. (2011) Control and characterization of individual grains and grain boundaries in graphene grown by chemical vapor deposition. *Nat Mater* 10:443–449.
24. Gao LB, et al. (2010) Efficient growth of high-quality graphene films on Cu foils by ambient pressure chemical vapor deposition. *Appl Phys Lett* 97:183109.
25. Gupta A, Chen G, Joshi P, Tadigadapa S, Eklund PC (2006) Raman scattering from high-frequency phonons in supported n-graphene layer films. *Nano Lett* 6:2667–2673.
26. Jiang L, et al. (2008) Organic single-crystalline ribbons of a rigid "H"-type anthracene derivative and high-performance, short-channel field-effect transistors of individual micro/nanometer-sized ribbons fabricated by an "organic ribbon mask" technique. *Adv Mater* 20:2735–2740.
27. Liao L, et al. (2010) Sub-100 nm channel length graphene transistors. *Nano Lett* 10:3952–3956.
28. Bai JW, et al. (2011) Top-gated chemical vapor deposition grown graphene transistors with current saturation. *Nano Lett* 11:2555–2559.
29. Wu W, et al. (2011) Growth of single crystal graphene arrays by locally controlling nucleation on polycrystalline Cu using chemical vapor deposition. *Adv Mater* 23:4898–4903.
30. Ji HX, et al. (2011) Graphene growth using a solid carbon feedstock and hydrogen. *ACS Nano* 5:7656–7661.
31. Li XS, et al. (2010) Graphene films with large domain size by a two-step chemical vapor deposition process. *Nano Lett* 10:4328–4334.
32. Liu LX, et al. (2012) A systematic study of atmospheric pressure chemical vapor deposition growth of large-area monolayer graphene. *J Mater Chem* 22:1498–1503.